Journal of Thermal Analysis, Vol. 52 (1998) 523-535

Al–Zn–Sn PHASE DIAGRAM
X-ray diffraction study at various temperatures

E. Aragon and A. Sebaoun

Laboratoire de Physico-Chimie du Matériau et du Milieu Marin, Matériaux à Finalité Spécifique (E.A. 1356), Université de Toulon et du Var, B.P. 132, 83957 La Garde Cedex France

(Received November 25, 1997)

Abstract

Further studies of the ternary phase diagram Al–Zn–Sn have been carried out by X-ray diffraction at various temperatures and by thermodilatometry in order to confirm our earlier experimental results which have been refuted by some recent work based on thermodynamic optimization. These new results, in particular the change with temperature of the crystallized fraction for Al–Zn–Sn mixtures containing up to 31.5 mass% of tin, confirm our previous results on the existence of a significant retrograde miscibility of tin in a solid solution α'_{ss} (in the temperature range 286 to 335°C) which protrudes into the ternary system starting from the Al–Zn binary up to a tin concentration of about 50 mass%. This disagreement between theory and experiment highlights the difficulties of a thermodynamic optimization approach based on solid state solubilities in the binary systems and on ternary liquidus data which disregards the ternary interaction parameters in the solid state. Besides, this experimental study highlights the difficulties in understanding the phenomena which depend on phase stabilities.

Keywords: phase diagram, retrograde miscibility, ternary system Al–Zn–Sn, thermodilatometry, X-ray diffraction at various temperatures

Introduction

The Al–Zn binary phase diagram [1] (Fig. 1) reflects an eutectic system involving a monotectoid reaction and a miscibility gap in the solid state. The aluminium solid solution has an extended homogeneity range, interrupted at lower temperatures by the miscibility gap. This solid solution is labelled α_{ss} on the Al-rich side (α_{ss} is a f.c.c.(A1) solid solution) and α'_{ss} on the Zn-rich side (α'_{ss} has a rhombohedral structure which corresponds to the α_{ss} structure, where one of the ternary axes has been slightly stretched).

Previous studies of the Al–Zn–Sn phase diagram were incomplete and agreed only on the existence of two invariant ternary reactions [2 to 9]. A more recent in-

1418–2874/98/ $ 5.00

Akadémiai Kiadó, Budapest
Kluwer Academic Publishers, Dordrecht

vestigation, based on calorimetric measurements [10], has confirmed the studies of the liquidus, although the extrapolation in the ternary system, based on much debated bibliographic data on the binaries, appears to be of little significance in determining the solid–solid equilibria.

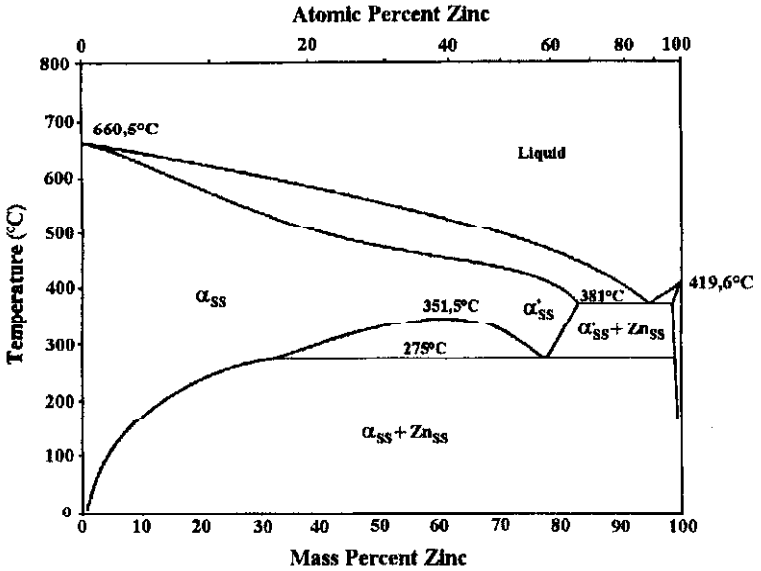

Fig. 1 Al–Zn binary phase diagram from [1]

In previously published papers ([11 to 17]), we have proposed a phase diagram (Fig. 2a) showing all liquid–solid and solid–solid equilibria. In those papers, the stability fields of the phases in equilibrium as well as the ternary isobaric invariants have been determined or more accurately investigated (Fig. 2b–d). Studies have been made by the isopleth cutting method using coupled direct and differential thermal analysis, metallographic observations, electron probe microanalysis and examining the phases formed by isothermal diffusion in the ternary system.

Figures 2b, 3 and 4 show the existence of a solid solution α'_{ss} extending in the direction of high concentration of tin, exhibiting an important retrograde miscibility for tin. On each side of the solid solution, for zinc concentrations varying from 30 to 99 mass% and temperatures higher than about 286°C, two solid–solid dual phase fields correspond to:

$$\alpha'_{ss} + \alpha_{ss} \qquad \text{and} \qquad \alpha'_{ss} + Zn_{ss}$$

With liquids, these solid phases give the three-phase fields:

$$L + \alpha'_{ss}, \qquad L + \alpha'_{ss} + Zn_{ss}, \qquad L + \alpha'_{ss} + \alpha_{ss}$$

These correspond in Fig. 2c to the monovariant lines which converge at 278°C. At this temperature an invariant reaction occurs which is a transitory peritectic [17 to 21]:

$$L + \alpha'_{ss} \rightleftharpoons Zn_{ss} + \alpha_{ss} \qquad \Delta H^{\circ} < 0$$

where ΔH° is the enthalpy.

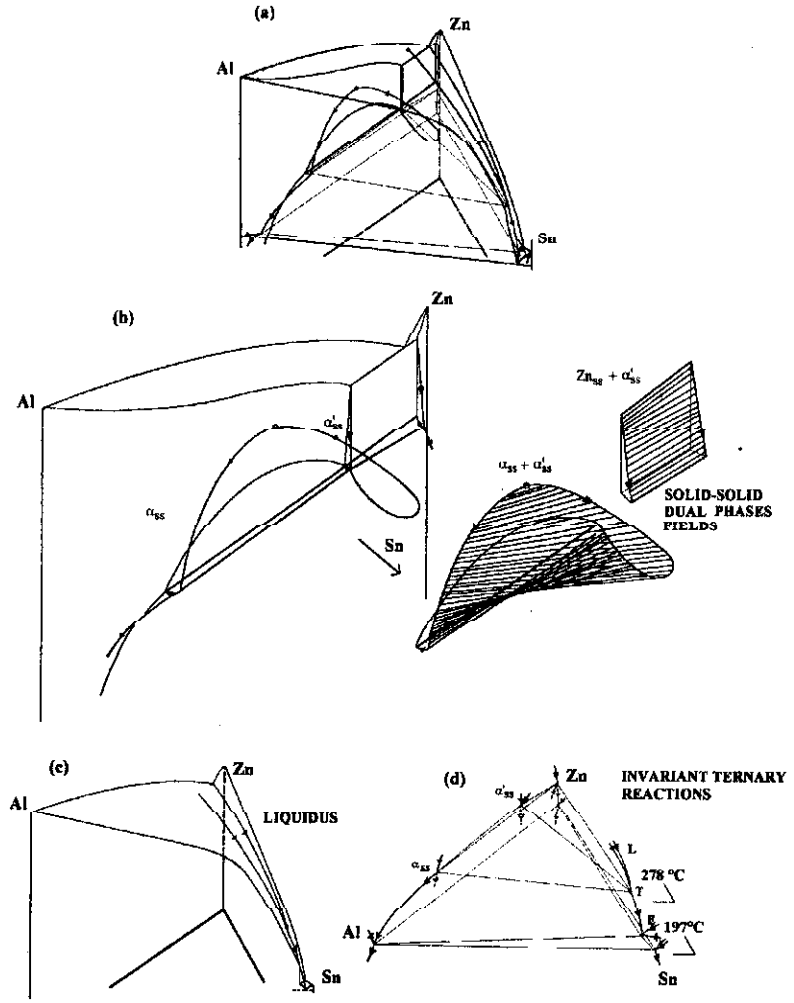

Fig. 2 Al–Zn–Sn phase diagram: (a) complete diagram; (b) solidus area: solid solution showing retrograde miscibility of tin, critical point (446°C) on α_{ss}–α'_{ss} solid solution miscibility gap (perspective view); (c) liquidus area with monovariant curves, one of which exhibits a vanishing point (446°C) conjugated with the solid–solid critical point (perspective view); (d) invariant ternary reactions: eutectic (E) at 197°C, transitory peritectic (T) at 278°C, liquidus (L) (perspective view)

Recently, for Fries *et al.* [22] our results have seemed to be thermodynamically impossible. Hubert *et al.* [23] have used Fries' argumentation and data. They proposed isothermal sections calculated from the parameters given by Fries [22]. Hence, it became necessary to confirm our earlier results by other experimental methods.

Experimental

An X-ray diffraction powder method was used with $CuK_{\bar{\alpha}}$ radiation (λ = 0.15405 nm) at different temperatures ranging from room temperature up to 400°C. An ANTON-PAAR HTK10 high temperature camera was employed on the PHILIPS PW 1050/20 goniometer. The experiments were carried out under inert gas (helium). The thermal sequences and the goniometer $\theta/2\theta$ scanning were computer assisted. A computer program permits also the acquisition and treatment of X-ray diffraction data [24].

The samples were prepared by weighing and mixing pure Al, Zn and Sn (99.999%), melting and dropping on a cold sheet to obtain a thin homogeneous foil. To take into account any preferred orientation of the crystallites, we have compared the X-ray spectra of annealed foils with those of powders obtained by grinding at liquid nitrogen temperature.

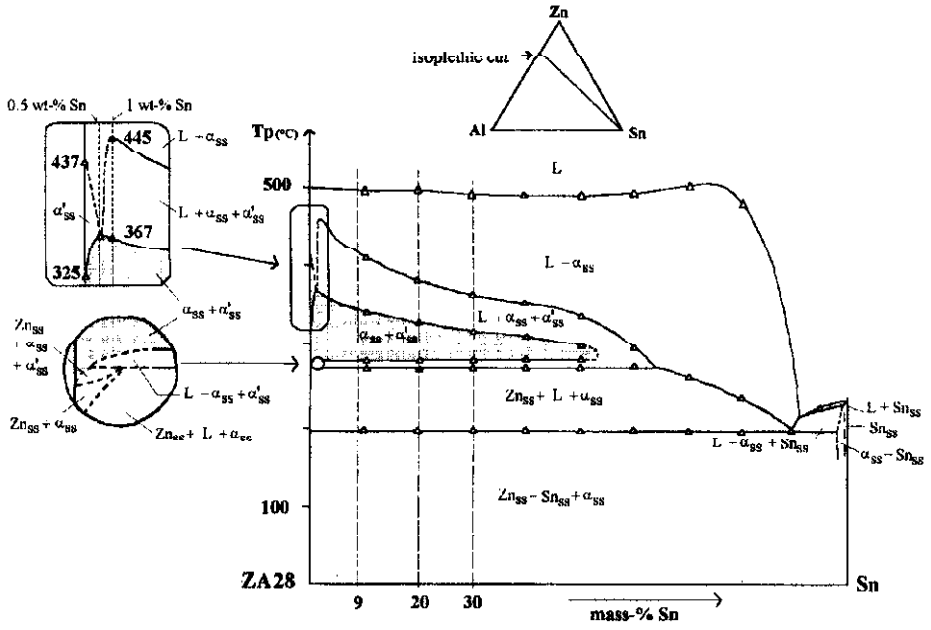

Fig. 3 Al–Zn–Sn phase diagram: isoplethic cut ZA28-Sn. Temperatures obtained by DTA [12]

To correct the thermal gradient between the upper side of the sample and the indication given by the thermocouple which controls the thermal regulation of the platinum heating rod and which indicates the sample temperature [25], we had to calibrate these temperatures in the range of study (25 to 400°C) by determining the melting point of high purity Sn and Zn. This calibration needed very slow heating, X-ray diffraction recording by steps of 1°C near the melting temperature and annealing times of 15 min or each step.

Preliminarily, a direction-finder calibration of the goniometer was carried out. In order to estimate the θ shift with temperature due to thermal dilatation, a θ calibration was also conducted with high purity aluminium, zinc and tin at different temperatures. The maximal precision after the calibration for the present results are: ±1°C for temperature; $\pm 3 \cdot 10^{-3}$ for lattice parameter.

Three different compositions (9, 20, 30 mass% of tin) on the isoplethic cut ZA28-Sn (m_{Al}/m_{Al+Zn}–0.28) (Figs 3 and 4) and another one (31.5 mass% of Sn) on the isoplethic cut ZA35-Sn (Fig. 4) were analysed by X-ray diffraction at different temperatures. Between 260 and 360°C, X-ray recording was carried out by steps of 5°C. Acquisition was preceded by an initial annealing time of 20 min for each step. Hence, the total annealing time (initial annealing plus θ-scanning time) was 50 min. To prevent metastable equilibria, some experiments were conducted using a long annealing time (24 h). Several experiments were recorded for each sample and compared.

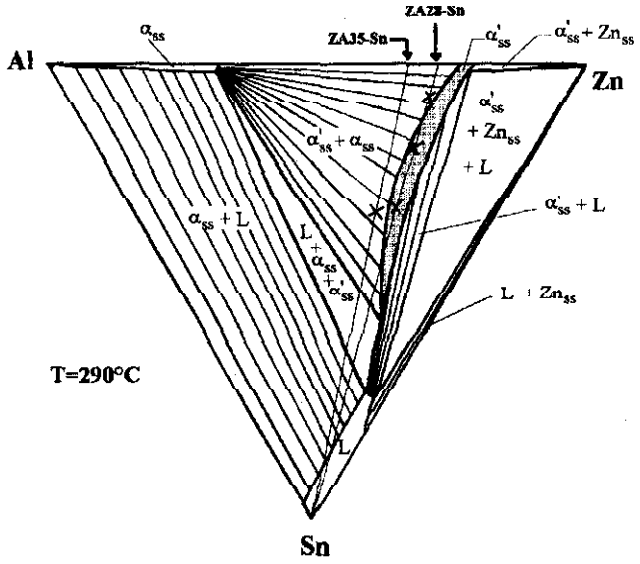

Fig. 4 Al–Zn–Sn phase diagram: 290°C isotherm deduced from electron probe microanalysis of the phases formed by isothermal diffusion [17]. X: compositions of the mixtures studied by X-ray diffraction

The literature gives, at 25°C, the X-ray diffraction patterns for high purity aluminium [26], zinc [26] and tin [27]. The identification of the corresponding solid solutions at different temperatures is done by extrapolation from these room temperature data. X-ray diffraction data are available for the binary α'_{ss} solid solution [28]. These authors worked on a quenched aluminium-(29 at.%) zinc binary alloy and identified a metastable transition phase which has a trigonal deformed Al (f.c.c.) structure. We have observed similar spectra at different temperatures for a binary aluminium-(38 at.%) zinc alloy (in the α'_{ss} one phase field between 275 and 400°C). These spectra have been our references for the identification of the α'_{ss} solid solution diffraction lines in the ternary alloys.

In any case, in any comparison with reference data, the θ shifts due to thermal dilatation and solubility variation with temperature have to be taken into account.

In order to confirm the results obtained by X-ray diffraction at various temperatures, we have carried out dilatometric measurements using an ADAMEL DI.20 dilatometer. A dilatometric curve has been recorded for a 20 mass% Sn sample on the isopleth ZA28-Sn between room temperature and 340°C at a heating rate of 5°C min^{-1}. The samples were cylindric rods (L_o=40 mm, D_o= 5 mm) previously loaded (ΔL_o=100 μm) by the sensor in the length direction.

Results

X-ray diffraction at various temperatures

Results have been considered on both heating and cooling because of nucleation difficulties during crystallization on cooling. In addition, preferential crystal orientations in solid–liquid fields were observed which modify Bragg lines intensities. Results concerning the 9 mass% Sn mixture have not been presented, because for this low tin content, the amount of liquid when this phase exists, is not large enough to observe a significant difference from the results for a completely solid phase. The results are summarized in Figs 5 to 8.

First, Fig. 5 shows a spectra selection: between 19 and 23 degrees in θ-Bragg angles, we can see the main diffraction lines.

On heating (Fig. 5A) we observed that, between the 277 and 282°C isotherms, the invariant reaction occurs (at 278°C [12]):

$$\alpha_{ss} + Zn_{ss} \rightleftharpoons \alpha'_{ss} + L \qquad \Delta H^\circ > 0$$

Then, we followed the variations in the intensities of the diffraction lines (the vertical scale is normalized to the highest diffraction line each spectrum) with temperature, and observed a diminution of the diffuse background intensity *vs.* the Bragg diffraction lines in the temperature range 290–320°C. This temperature range varied with the tin content but the phenomenon was observed for all

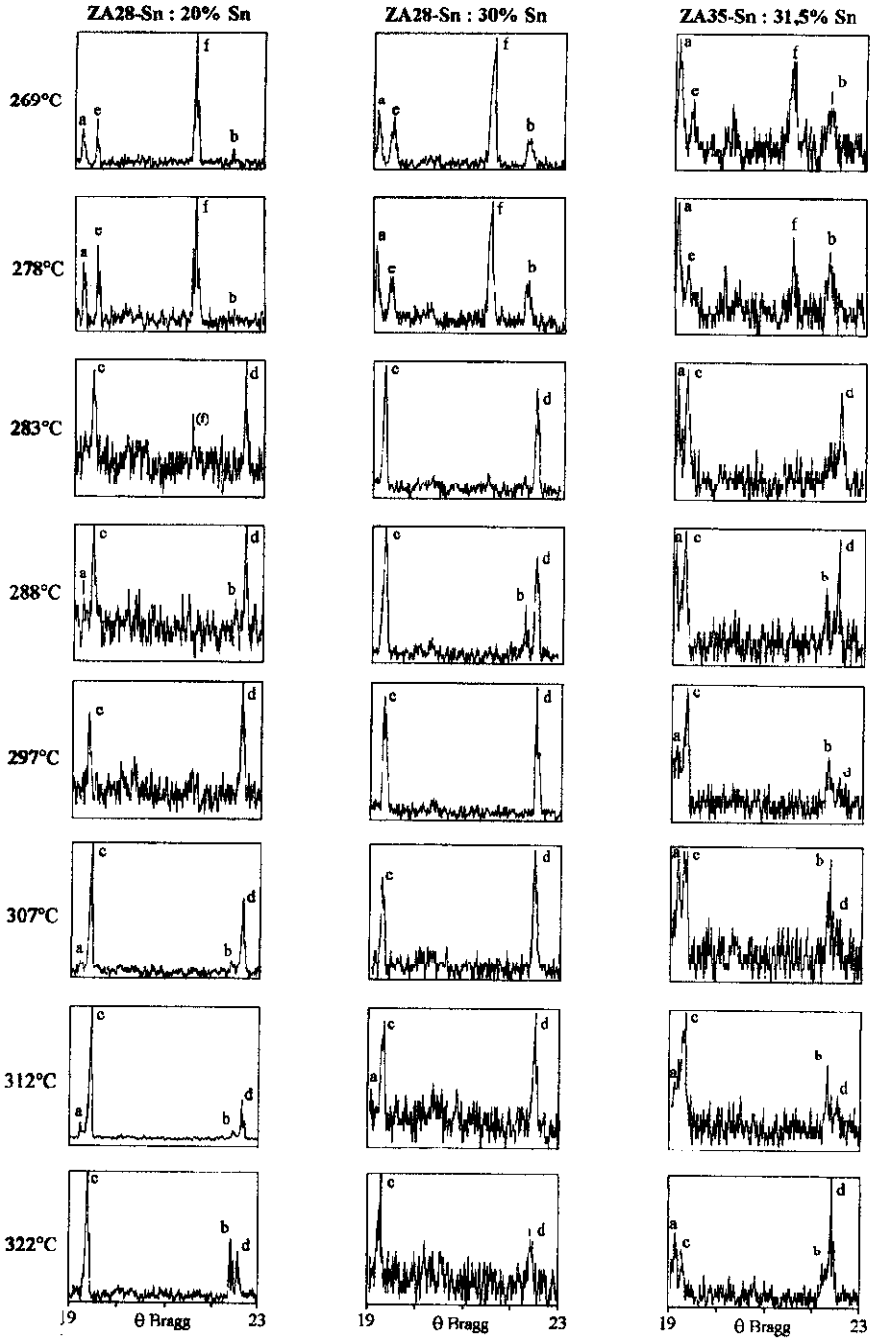

Fig. 5A X-ray diffraction spectra selection on heating. Notation of the diffraction lines: a≡α_{ss}(111); b≡α_{ss}(200); c≡α'_{ss}(101); d≡α'_{ss}(012); e≡Zn_{ss}(100); f≡Zn_{ss}(101)

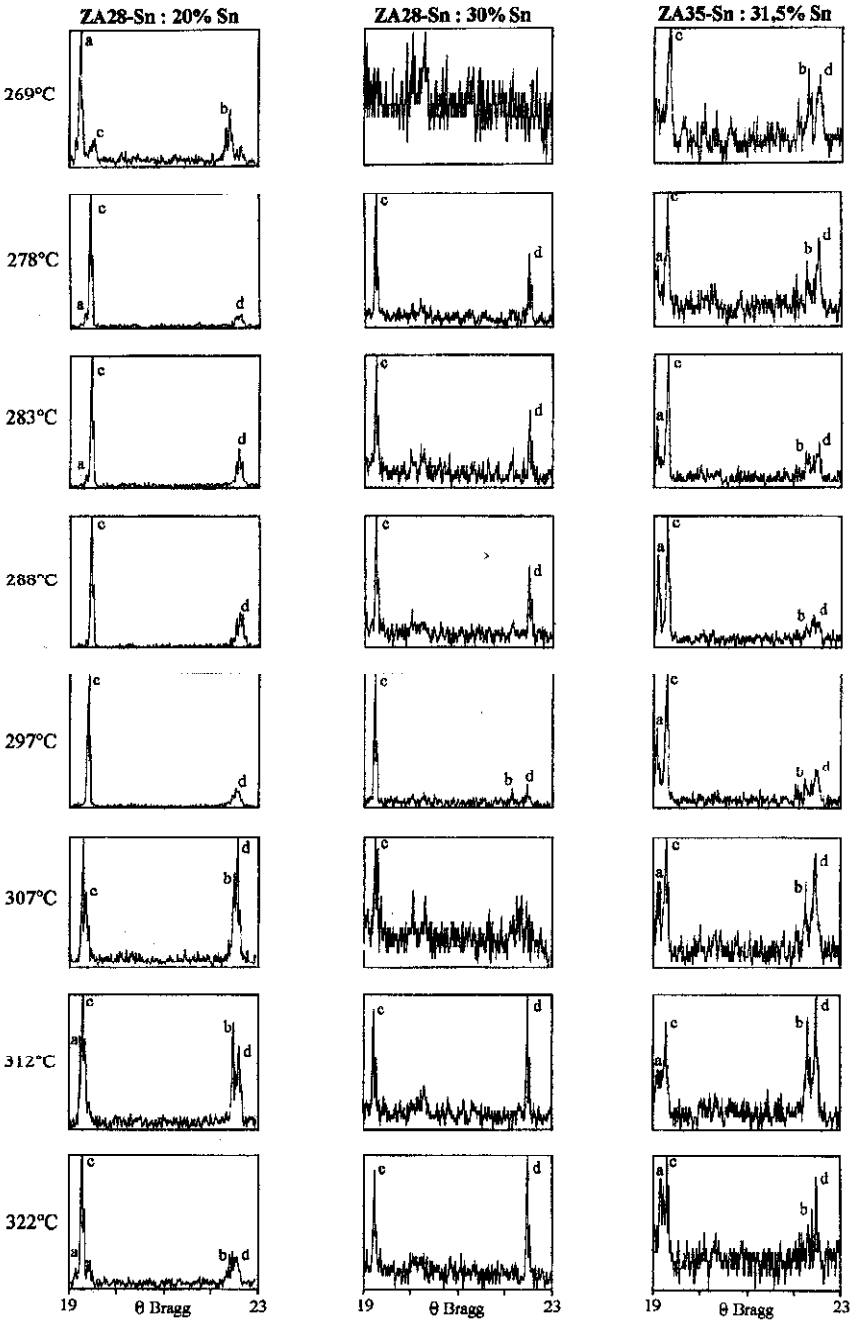

Fig. 5B X-ray diffraction spectra selection on cooling. Notation of the diffraction lines: $a \equiv \alpha_{ss}(111)$; $b \equiv \alpha_{ss}(200)$; $c \equiv \alpha'_{ss}(101)$; $d \equiv \alpha'_{ss}(012)$

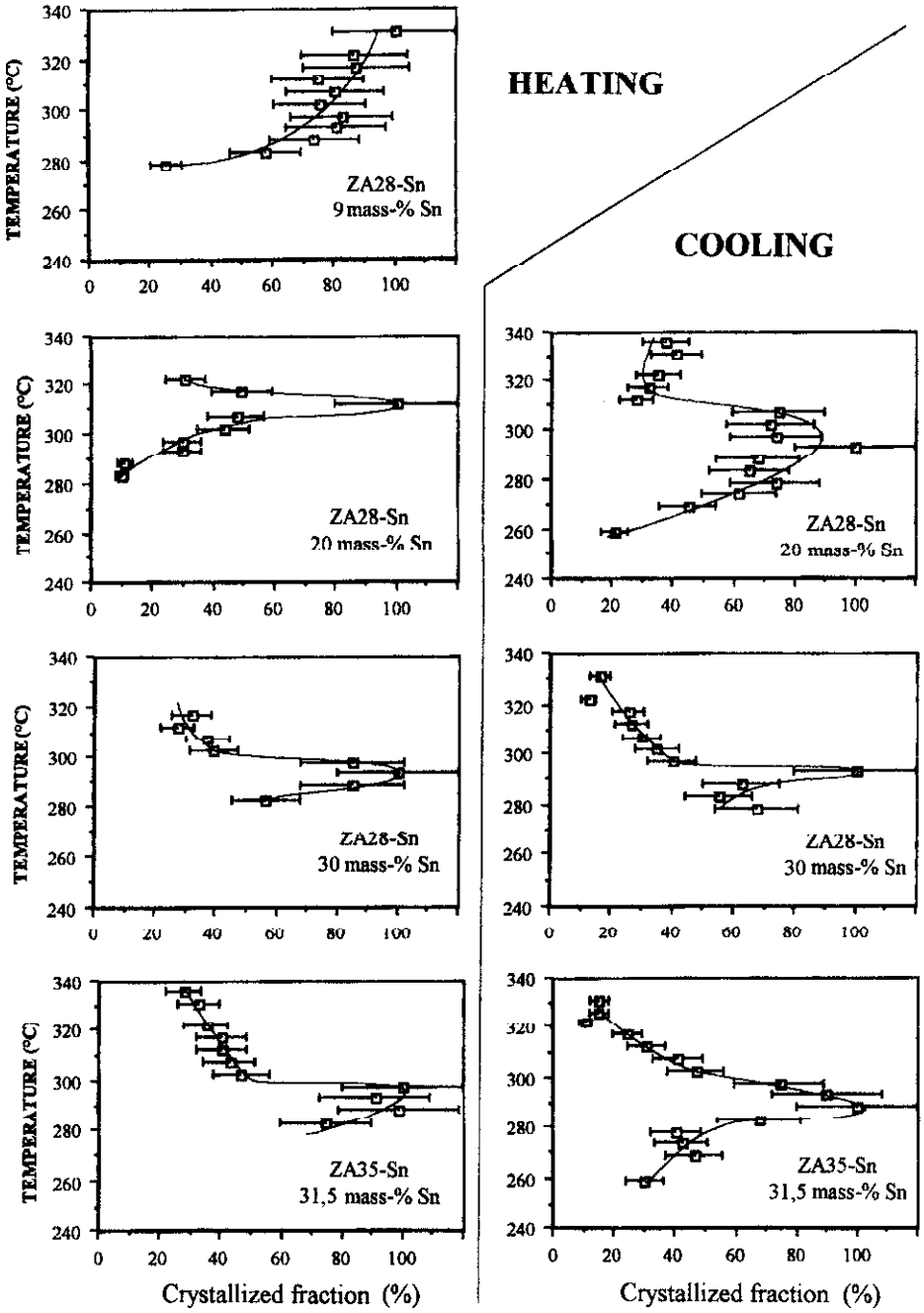

Fig. 6 A mean crystallized fraction (based on the α'_{ss} diffraction lines 101, 012 and 110) as a function of temperature on heating and cooling

mixtures. It should be mentioned that, depending on the composition, either the $\alpha_{ss}+\alpha'_{ss}$ dual phase field (sample of 9 mass% Sn on the isopleth ZA28-Sn and 31.5 mass% Sn on the isopleth ZA35-Sn) or the α'_{ss} one phase field (samples of 20 and 30 mass% Sn on the isopleth ZA28-Sn) (Fig. 4) is observed. For the last three compositions, alloys can pass in either of the two solid phase fields depending on the temperature because of the curvature of the boundary between the two solid phase fields in the ternary phase diagram.
In cooling experiments (Fig. 5B), the results were in a good agreement with those obtained on heating.

Figure 6 shows the change of the crystallized fraction with temperature for different tin concentrations. Here, we have followed the mean ratio S_c/S_m where S_c is the diffraction line area (corrected for the background area), divided by S_m (S_m is the maximum value of S_c). We have represented the average of this ratio for the three main diffraction lines of the solid solution α'_{ss} in order to cancel the crystal orientation effects due to the existence of a liquid phase in some fields. A maximum is noticed which corresponds to the solid phase field in the temperature range 290 to 320°C. It corresponds to a solid phase field inside a liquid–solid phase field.

Figure 7 shows the change in inter-reticular distances with temperature for a mixture with 31.5 mass% of tin on the isopleth ZA35-Sn. On heating, the transitory peritectic invariant reaction is characterized by the disappearance of the zinc diffraction line (100), the emergence of the α'_{ss} (101) line and by a discontinuity in the α_{ss} (111) change. On cooling, the discontinuity of the reticular distance $d_{\alpha'(101)}$ points to a phase field boundary associated with an important change in the composition of the solid solution α'_{ss} at about 280°C. The peritectic invariant reaction does not appear because of a temperature shift between the heating and the cooling data.

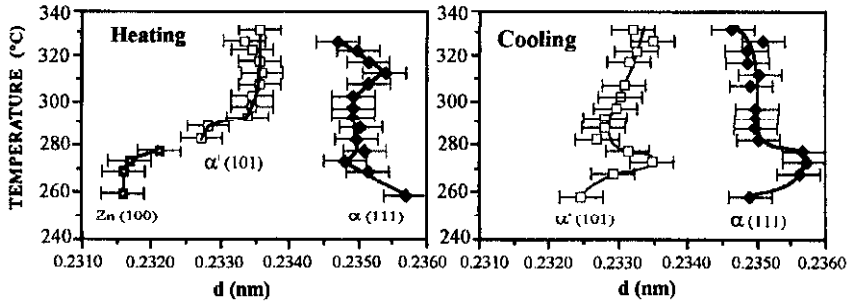

Fig. 7 Change in inter-reticular distances with temperature for a mixture with 31.5 mass% of tin on the isoplethic cut ZA35-Sn

Isothermal representation (Fig. 8) of the change in inter-reticular distances at 293°C (temperature for which we observe maximum crystallization in Fig. 6) shows a linear growth with tin composition on the isopletic cut ZA28-Sn for the

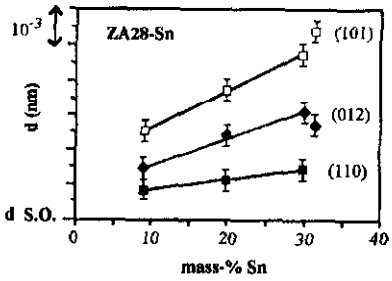

Fig. 8 Change in isothermal inter-reticular distances with tin content at 293°C for the α'_{ss} diffraction lines (101), (012) and (110). *d Scale Origin*=0.2280 nm: α'_{ss}(101), 0.1985 nm: α'_{ss}(012), 0.1410 nm: α'_{ss}(110)

α'_{ss} diffraction lines (101), (012) and (110). This result would correspond to a tin miscibility in the solid solution α'_{ss} up to 30 mass%. With regard to the 31.5 mass% Sn sample, the discontinuity of the curves would correspond to the crossing from the α'_{ss} one phase field to the α_{ss}+α'_{ss} dual phase field. Then, the Sn miscibility in the α'_{ss} solid solution seems to change and to become variable with solvus path.

Thermodilatometry

The results of the thermodilatometric study are presented in Fig. 9 for a 20 mass% Sn sample on the isoplethic cut ZA28-Sn.

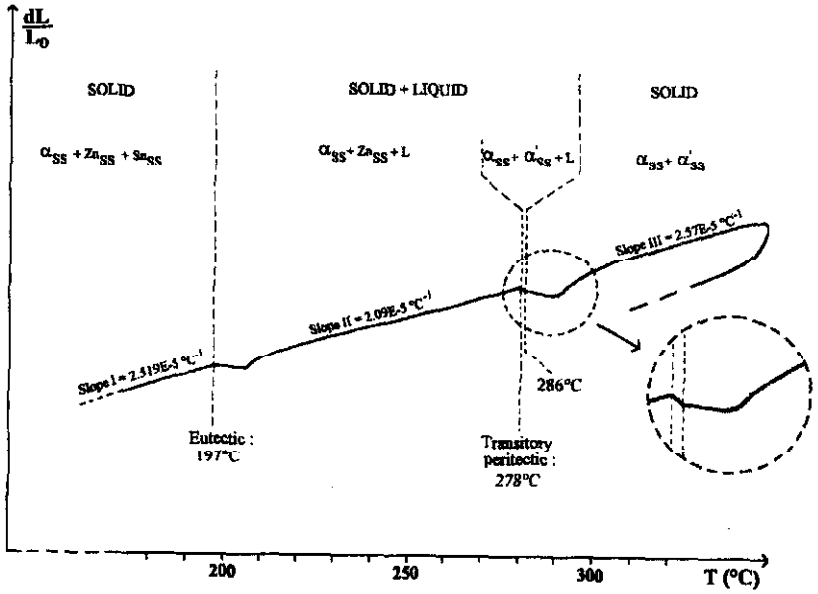

Fig. 9 Thermodilatation curve for a 20 mass% Sn sample on the isopleth ZA28-Sn

For a field containing both liquid and solid, the coefficient of linear expansion (or the slope of the dilatation curve) is expected here to be smaller than for a solid field because the three-dimensional flow of the liquid under sensor compression diminishes the linear thermal dilatation. For part II (eutectic liquid+solid), the slope is in fact smaller than for part I, which is known to correspond to a solid field. For part III (above 286°C), we have observed a slope which is even larger than for part I: this shows that part III would correspond to a solid field, which, from our other experiments, is the $\alpha_{ss}+\alpha'_{ss}$ field.

Conclusions

This experimental study based on X-ray diffraction at different temperatures and thermodilatometry, completes our previous results [13, 15, 17] obtained by coupled direct and differential thermal analysis, microprobe analysis, calorimetric studies and diffusion path determinations.

On the one hand, our different experiments show very complex phenomena for which we cannot propose any other interpretation than the existence of an α'_{ss} ternary solid solution exhibiting towards tin a large retrograde solubility, even if we are aware of the possible appearance of non-equilibrium phases. On the other hand, the critical assessment [22, 23] based on thermodynamic modelling cannot easily describe such a complex phenomenon.

* * *

The authors thank the D.G.A./D.C.N. (Délégation Générale de l'Armement/Direction des Constructions Navales) of Toulon for financial support during the thesis preparation of E. Aragon at Toulon University. In particular, the help of Mr. Giroud is gratefully acknowledged

References

1 J. L. Murray, Bull. Alloys Phase Diagrams, 4 (1983) 55.
2 D. V. Plumbridge, On the binary and ternary alloys of Al, Zn, Cd and Sn, Thesis, University of München, Germany, 1911.
3 E. Crepaz, Giorn. Chim. Ind. Appl., 5 (1923) 115.
4 L. Losana and E. Carozzi, Gazetta Chim. Ital., 53 (1923) 546.
5 H. Nishimura and O. Suzuki, Suiyokwai-Shi (Trans. Min. Metall. Assoc., Kyoto), 4 (1925) 1441.
6 V. Jares, Am. Inst. Min. Metall. Eng., (oct. 1926) 1.
7 S. Prowans and M. Bogatyrevicz, Zavod. Lab., 35 (1969) 62.
8 S. Prowans and M. Boratyrevicz, Arch. Hutn., 13 (1968) 217.
9 A. A. Tikhomirov, B. M. Lepinskikh, I. T. Sryvalin and V. G. Korpachev, Zh. Fiz. Khim., 42 (1968) 723.
10 A. K. Nayak, Trans. Indian Inst. Met., 28 (1975) 148.
11 A. Sebaoun and A. Vincent, Communication à la 6ème Journée d'Etude des Equilibres entre Phases, Nancy, 1980.
12 D. Vincent, D.E.S., No. 84, Université Claude Bernard, Lyon I, France, 1980.

13 D. Vincent and A. Sebaoun, J. Thermal Anal., 20 (1981) 419.
14 D. Vincent and A. Sebaoun, Mém. Etud. Sci. Rev. Métall., 78 (1981) 165.
15 D. Vincent, Contribution to the Study of the Ternary Al-Zn-Sn system, Thesis, No. 81, Université Claude Bernard, Lyon I, France, 1982.
16 A. Sebaoun, D. Vincent and A. M. Zahra, Conference on Chemical Thermodynamics IUPAC., University College, London 1982.
17 A. Sebaoun, D. Vincent and D. Treheux, Mater. Sci. Techn., 3 (1987) 241.
18 R. Cayron, Etude et Théorie des Diagrammes d'Equilibre dans les Systèmes Quaternaires, Vol. 1, Louvain, Belgium, Institut de Métallurgie, 1960, p. 15.
19 A. P. Rollet and R. Bouaziz, L'Analyse Thermique, Vol. 1, Gauthier Villars ed., Paris 1972, p. 34.
20 J. Postma, Rec. Trav. Chim., 39 (1920) 515.
21 F. N. Rhines, Phase Diagrams in Metallurgy: their Development and Application, New York, Mc Graw-Hill ed., 1956, p. 176.
22 S. G. Fries, H. L. Lukas, S. Kuang and G. Effenberg, Assessment of the Al-Zn-Sn System, in User Aspects of Phase Diagrams, F. Hayes ed., The Institute of Metals, London, 1991, 280
23 M. Hubert-Protopopescu and H. Hubert, Ternary Alloys, Vol. 8, G. Petzow and G. Effenberg V.C.H. ed., 1993, p. 381.
24 H. A. J. Oonk, Phase Theory: The Thermodynamics of Heterogeneous Equilibria, Elsevier ed., 1981, p. 80.
25 B. Ducourant, R. Fourcade and G. Mascherpa, Licence C.N.R.S./A.N.VA.R., marketed by Philips.
26 N. E. Brown, S. M. Swapp, C. L. Bennet and A. Navrotsky, J. Appl. Cryst., 26 (1993) 77.
27 Swanson and Tatge, Natl. Bur. Stand. (U.S.), Circ. 539, 1 (1953) 11.
28 J. D. Barnett, R. B. Bennion and H. T. Hall, Science, 141 (1963) 1041.
29 K. K. Rao, H. Herman and E. Parthé, Mater. Sci. Eng., 1 (1966) 162.